Universidad Autónoma de San Luis Potosí
Instituto de Física
"Manuel Sandoval Vallarta"

Un arreglo teórico-experimental para la determinación de movilidades electroforéticas

Tesis presentada por:

Carmen Lucía Moraila Martínez

para obtener el grado de

Maestro en Ciencias (Física)

Asesores de tesis:

Dr. Enrique González Tovar

Dr. Guillermo Iván Guerrero García

San Luis Potosí, San Luis Potosí, México

Enero 2018

Contents

CHAPTER 1

Introduction

The behaviour of colloidal particles and their interactions is a classic research subject in physical-chemistry . The attainment of a faithful description of the behaviour of small particles has been, for many years, the goal of numerous fundamental studies and of relevance for uncountable technological applications, e.g., in biology, energy and the environmental sector.

In surface science (*1*), a colloid is any particle that has some linear dimension between 10^{-9} m (10 $\mathring{A}$) and 10^{-6}m (10 μm), see Figure 1.1. Additionally, large molecules or finely subdivided bulk matter can also be considered colloids if they are formed by particles in the spatial range of 10^{-9} to 10^{-6} m. Thus, in the thermodynamic sense, macromolecular colloids are true solutions. Subdivided bulk matter, on the other hand, forms a two-phase (at least) system with the medium. The difference between macromolecular colloids and subdivided bulk matter is the relationship that exists between the colloidal particle and the medium in which it is embedded.

Due to the wide definition of colloids, they comprise an extensive multitude of material systems of great interest (Figure 1.2) in scientific and technological fields (*1–4*). One conspicuous example of a complex fluid is petroleum.

As result of the impressive progress that molecular engineering has experienced over the past several years, diverse colloidal systems (liquid crystals, biomaterials, colloidal crystals) have been

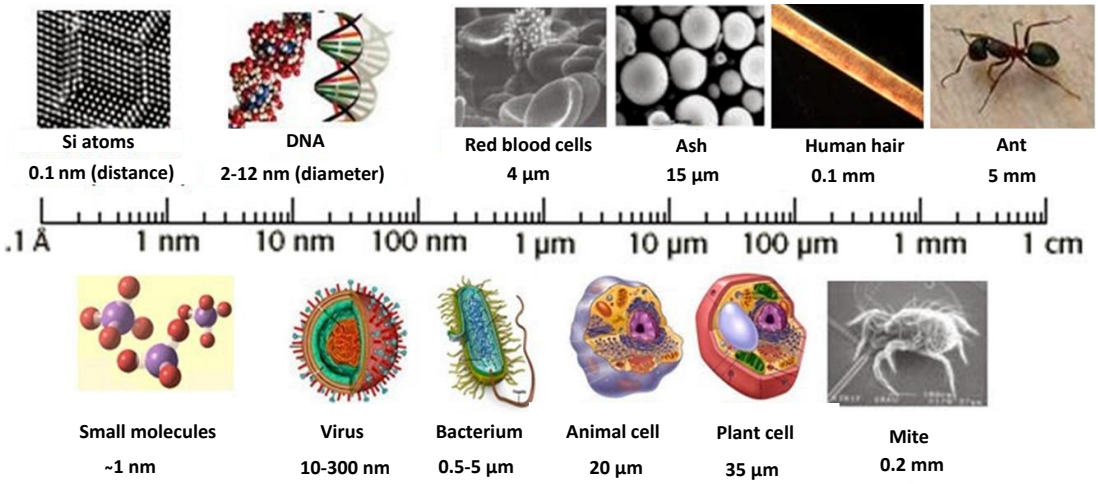

Figure 1.1: Scales sketch of different colloids.

			Examples		
Medium	*Particle*	*Name*	*In Nature*	*Biological*	*Technical*
Liquid	Solid	Colloidal sol	River water, glacial runoff, muddy water		Paint, ink Sol–Gel Processing
Liquid	Liquid	Emulsion (nonequilibrium) solution (equilibrium)		Fat digestion, biological membranes	Drug delivery, emulsion polymerization
Liquid	Gas	Foam	Polluted rivers	Vacuoles, insect excretions	Fire extinguishers, production of porous plastics
Gas	Solid	Aerosol	Volcanic smoke	Pollen	Inhalation of solid pharmaceuticals
Gas	Liquid	Aerosol	Clouds	Result of coughing	Hair spray, smog
Solid	Solid	Solid suspension	Wood	Bone	Composites
Solid	Liquid	Porous material	Oil reservoir rock, opals	Pearl	High impact plastics
Solid	Gas	Solid foam	Pumice	Loofah	Styrofoam, zeolites

Figure 1.2: Diverse types of colloidal systems (dispersions).

successfully used, for instance, in display fabrication for medicine and optoelectronic applications (see Figures 1.3 and 1.4).

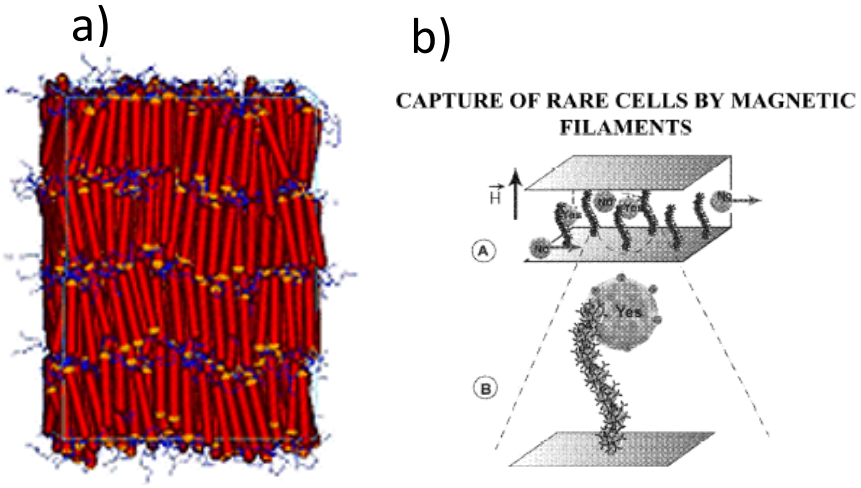

Figure 1.3: (a) Crystal liquid and (b) Magnetic colloid application in medicine.

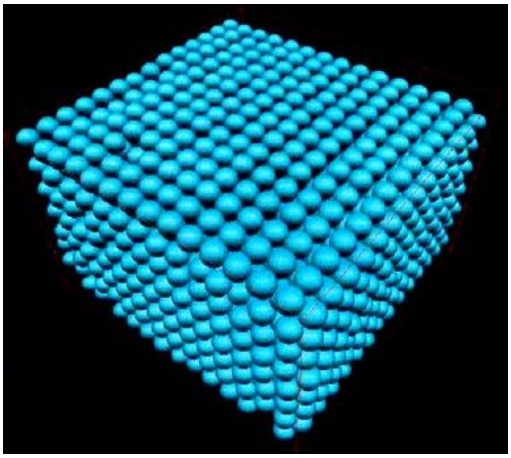

Figure 1.4: Photonic crystal.

Usually, colloids are dispersed in a solvent, and frequently the liquid is a polar substance (such as water). Tipically, a dissolved macroparticle acquires an electrical charge due to the adsorption/desorption of ions on its surface. When the particle is in suspension, and due to its electrical charge, the combined effect between Coulomb forces and thermal agitation of the free ions dispersed in the fluid produces an Electric Double Layer (EDL). The EDL is a physicochemical key concept which refers to the atmosphere created by the ionic distribution of an electrolyte around an electrically charged colloid or surface (see Figure 1.5).

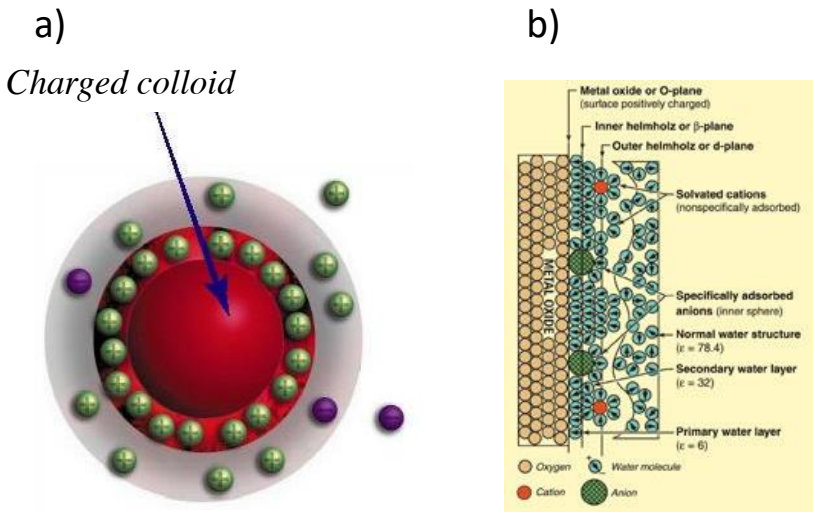

Figure 1.5: (a) Simple representation of the Electric Double Layer and (b) detailed model of the interface.

Since the past century, the EDL has been investigated by means of experiments, theoretical models and computer simulations. However, the detailed information about the charge density profiles is not easily accessible to direct measurements. On the other hand, the most fundamental theories and computer simulations of the EDL can provide, fortunately, the primordial quantities of the problem, that is, the ionic distribution functions.

The point-ions model of an electrolyte has been the basis of the celebrated Gouy-Chapman theory and, in general, of the Poisson-Boltzmann (PB) description of the EDL, however, since the 1980s, a huge quantity of evidences has proved that the PB formalism has notable deficiencies because of its neglect of the very relevant ionic-size correlations. As a consequence, the simplest PB theory (i.e., without a "Stern layer") is unable to predict the novel phenomenon of charge reversal (*5*). Charge reversal is a recently reported "anomaly", which corresponds to the unexpected inversion of the polarity of the effective colloidal charge (viz., that including the native macroparticle charge plus that of the adsorbed ions) and, in the past years, this fascinating phenomenon have mustered a great deal of scientific interest in the literature ((*6*, *7*)). Notably, steric effects (that is, ionic-size correlations) have been started to be included in EDL approaches since two decades ago, mainly via modern integral equations theories for charged fluids (*6*). Along these lines, in the last years, diverse research groups have developed rigorous theoretical methods to describe the structural properties of EDL systems with different geometries. As an example, Guerrero et al.(*8*) found that valence is not the only relevant mechanism, but the differences in ionic sizes have to be also considered. These same authors investigated the totally asymmetric spheric (size and valence) EDL theory using the HNC/MSA integral equation, and found that, far

from the point of zero charge, the asymmetric EDL characteristics are not the same than those corresponding to a electrolyte of same charge and size of counterions (Figure 1.6).

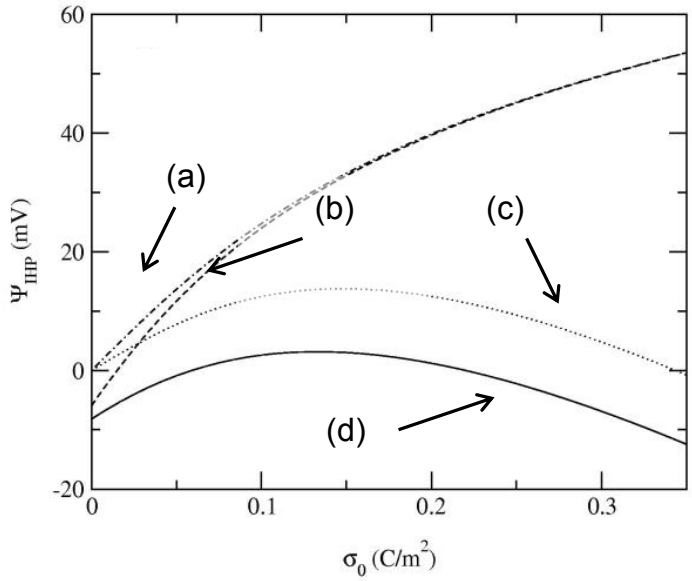

Figure 1.6: Potential in the Helmholtz plane as a function of the surface charge, for a totally asymmetric spherical EDL. Theories:(a) PB-Stern, (b) asymmetric PB Stern, (c) HNC/MSA same ionic size, (d) HNC/MSA different ionic size (*8*).

When an external electrical field is imposed to an equilibrium colloidal suspension an abundant collection of interesting transport processes arise. These relevant emerging effects include electrophoresis, streaming potentials, electroosmosis, etc (*1*, *9*). Among them, clearly, the most salient electrokinetic instance is that corresponding to the electrophoresis of macroparticles. As it is well-known, this nonequilibrium process consists in the motion of a charged colloid, immersed in a supporting medium (tipically an electrolytic solution), prompted by the force originated by the presence of the applied field. Electrophoresis is a paradigmatic technique of characterization and separation in biology (in the form of gel electrophoresis) and, in general, in surface science represents one of the methods par excellence to determine the stability/aggregation, charge and form of an enormous diversity of colloidal entities. From a fundamental perspective, the relevance of electrophoresis can be summarized by the words of Dukhin "...electrokinetic phenomena and, accordingly, the presence of surface charges in the boundary region between the liquid and the solid were the rule, rather than the exception, since practically every investigated inorganic and organic substance showed a charge on contact with a liquid, especially when the liquid was distilled water..." (*9*). Understandably, the quest for an adequate theoretical account of electrophoresis is a concurred and vintage problem in physical-chemistry. Nowadays, the most widely-accepted description of the colloidal mobility is that by O'Brien and White (*10*), which embodies the re-

tardation and relaxation contributions due to the distorted ionic cloud of a point-ions bathing electrolyte. In simple words, this approach obtains the electrophoretic velocity by solving, at a Poisson-Boltzmann level, the hydrodynamical equations associated to a colloidal suspension.

Recently, the Primitive Model Electrophoresis (PME) has been developed in the electrokinetics of coulombic fluids (*11*, *12*). PME allows to explain the electrophoretic mobility data in a wide range of ionic concentration, even for the case of colloidal suspension with multivalent electrolytes, improving the standard electrokinetic model of Wiersema, OBrien and White (*10*, *13*). Quesada et al. (*14*) have published an experimental data verification of the PME electrokinetics theory (see Figure 1.7).

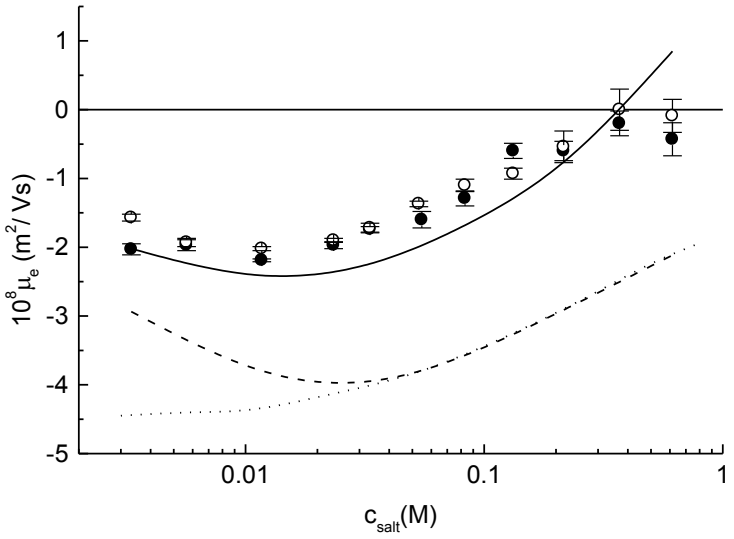

Figure 1.7: Electrophoretic mobility of a spherical colloid as function of 2:1 electrolyte concentration. Circles correspond to experimental data, continuous line to PME theory and dashed lines to punctual ion theory based in PB equation (*14*).

In the present dissertation, we describe the construction of an experimental setup for the measurement of electrophoretic mobilities of microparticles. We also validate and present preliminary results for the electrokinetic velocities of latex and silica colloids. These experimental data have been fitted via the well-known O'Brien and White theory of electrophoresis and, in addition, we report various derived colloidal properties such as the colloidal charge, and the surface and Helmholtz electrostatic potentials (described in Section 2). The work is divided in five chapters. The first is a brief introduction about colloids and their applications. In Chapter 2 the theoretical framework used to describe the equilibrium and transport properties of our system is presented. In Chapter 3, we explain the experimental arrangement used for the electrophoretic mobility measurements. In Chapter 4 the results obtained from experimental and their theoretical fitting are

exposed and discussed. Finally, a Conclusions and Forthcoming Research Chapter 5 is included.

CHAPTER 2

Theoretical framework

2.1 The classical Poisson-Boltzmann theory in planar geometry

Poisson-Boltzmann equation

Planar geometry

Let us consider a charged plate in the presence of a m-component electrolyte, as it is shown in Figure 2.1. The ionic cloud around the charged surface is the so-called the electrical double layer. In order to describe it, we start from the Poisson equation 2.1:

$$\nabla^2\phi(\vec{x}) = -\frac{\rho(\vec{x})}{\epsilon_0\epsilon_r} \tag{2.1}$$

where $\phi(\vec{x})$ and $\rho(\vec{x})$ are the mean electrostatic potential and the charge density per volume unit at position $\vec{x}$, respectively; ϵ_0 is the vacuum permittivity, and ϵ_r is the relative permittivity of the solvent e.g., $\epsilon_r = \epsilon_w/\epsilon_0 = 80$ for water at room temperature.

In planar geometry, the mean electrostatic potential and the ion distribution depend only on

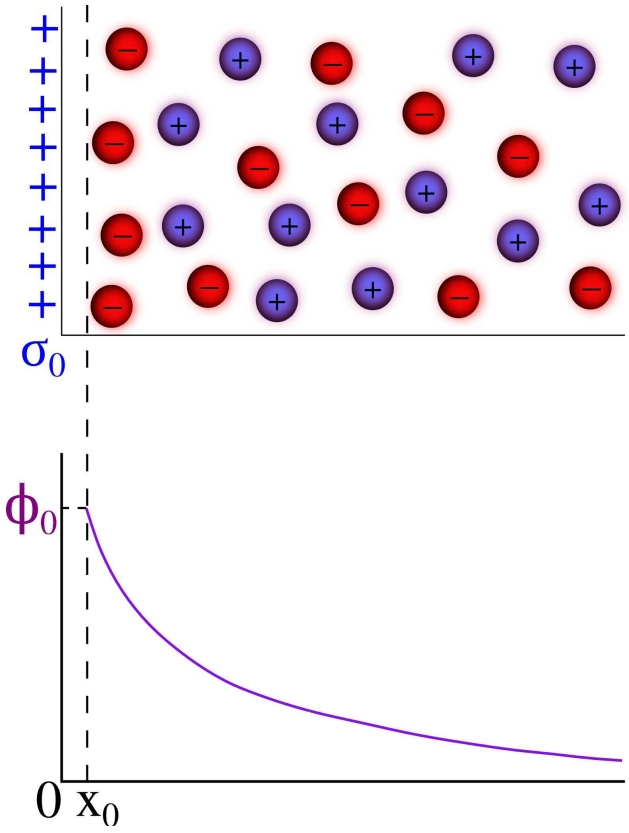

Figure 2.1: Schematic representation of the diffuse electrical double layer in planar geometry.

the distance to the charged plate. In this instance, the Poisson equation and charge density per volume unit can be written as:

$$\frac{d^2\phi(x)}{dx^2} = -\frac{\rho(\vec{x})}{\epsilon_0\epsilon_r} \tag{2.2}$$

$$\rho(x) = \sum_{i=1}^{m} n_i(x) z_i e_0 \tag{2.3}$$

with e_0 the magnitude of the electron charge, z_i the valence of ionic species i, and $n_i(x)$ the number of particles per volume unit as a function of the distance to the charge plate for the species i.

Formally, the number of particles per volume can be written as equation 2.4 (*15*, *16*)

$$n_i(x) = n_i^0 exp\Big(- \frac{W_i(x)}{k_B T}\Big), \tag{2.4}$$

where $n_i^0 = n_i(x \to \infty)$ is the value of the number ion density in the bulk electrolyte (far away from the charged plate), k_B is the Boltzmann constant, T is the temperature, and $W_i(x)$ is the so-called potential of mean force, which is the necessary work to bring an ion from the bulk electrolyte to the position x.

Let us approximate the potential of mean force by the electrostatic work required to bring an ion from the bulk electrolyte to the position x:

$$W_i(x) = (\phi(x) - \phi_\infty) e_0 z_i. \tag{2.5}$$

If the following boundary conditions are assumed

$$\phi_\infty = \lim_{x\to\infty} \phi(x) = 0, \tag{2.6}$$

and

$$\phi'_\infty = \lim_{x\to\infty} \frac{d\phi(x)}{dx} = 0, \tag{2.7}$$

the potential of mean force reduces to

$$W_i(x) = \phi(x) e_0 z_i. \tag{2.8}$$

Then, Eq. 2.4 can be written as

$$n_i(x) = n_i^0 exp\bigg(- \frac{\phi(x) e_0 z_i}{k_B T} \bigg), \tag{2.9}$$

which resembles to a Boltzmann factor. If Eq.2.9 is substituted in Eq.2.3 we obtain:

$$\rho(x) = \sum_{i=1}^{m} n_i^0 exp\bigg(- \frac{\phi(x) e_0 z_i}{k_B T} \bigg) z_i e_0. \tag{2.10}$$

Using Eq. 2.10 in Eq. 2.2, the Poisson-Boltzmann equation is obtained for planar geometry:

$$\frac{d^2\phi(x)}{dx^2} = - \frac{\sum_{i=1}^{m} n_i^0 z_i e_0 exp\bigg(- \frac{\phi(x) e_0 z_i}{k_B T} \bigg)}{\epsilon_0 \epsilon_r} \tag{2.11}$$

The linear Poisson-Boltzmann equation in planar geometry

For $\frac{\phi(x) e_0 z_i}{k_B T} < 1$, the exponential function can be approximated by its two first terms in a series expansion $e^x = 1 + x + \frac{x^2}{2!} + \frac{x^3}{3!} + ...$ to yield

$$\frac{d^2\phi(x)}{dx^2} = - \frac{\sum_{i=1}^{m} n_i^0 z_i e_0 + \sum_{i=1}^{m} n_i^0 z_i e_0 \bigg(- \frac{\phi(x) e_0 z_i}{k_B T} \bigg)}{\epsilon_0 \epsilon_r}. \tag{2.12}$$

Using the electroneutrality condition,

$$\sum_{i=1}^{m} n_i^0 z_i e_0 = 0, \tag{2.13}$$

it is possible to write the linearized Poisson-Boltzmann equation as

$$\frac{d^2\phi(x)}{dx^2} = \bigg(\frac{\sum_{i=1}^{m} n_i^0 z_i^2 e_0^2}{\epsilon_0 \epsilon_r k_B T} \bigg) \phi(x). \tag{2.14}$$

This equation is also known as the Debye-Hückel approximation, which can be also written as

$$\frac{d^2\phi(x)}{dx^2} = \kappa_D^2 \phi(x), \tag{2.15}$$

where κ_D is the Debye $k-$parameter

$$\kappa_D = \left(\frac{\sum_{i=1}^{m} n_i^0 z_i^2 e_0^2}{\epsilon_0 \epsilon_r k_B T} \right)^{1/2}. \tag{2.16}$$

The solution of Eq. 2.15 is of the form:

$$\phi(x) = constant \times exp(-\kappa_D x). \tag{2.17}$$

The Debye-Hückel approximation is a particular case of the non-linear Poisson-Boltzmann theory. This approximation is useful for weak surface charge densities of the charged plate.

The non-linear Poisson-Boltzmann equation in planar geometry

Interestingly, the non-linear Poisson-Boltzmann equation in planar geometry can be solved analytically for a binary charge symmetric electrolyte. In this instance, $z_+ = -z_- = z$ for a $z:z$ salt (e.g., NaCl or MgSO4). Also, $n_+^0 = n_-^0 = n^0$, which can be obtained from the bulk electroneutrality condition (see Eq. 2.13) for a binary electrolyte:

$$n_+^0 z_+ e_0 + n_-^0 z_- e_0 = 0. \tag{2.18}$$

Eq. 2.11 can be writen for a $z:z$ salt as

$$\frac{d^2\phi(x)}{dx^2} = -\frac{n_+^0 z_+ e_0 exp\left(-\frac{\phi(x) e_0 z_+}{k_B T} \right) + n_-^0 z_- e_0 exp\left(-\frac{\phi(x) e_0 z_-}{k_B T} \right)}{\epsilon_0 \epsilon_r}, \tag{2.19}$$

or

$$\frac{d^2\phi(x)}{dx^2} = -\frac{n^0 z e_0 exp\left(-\frac{\phi(x) e_0 z}{k_B T} \right) + n^0 (-z) e_0 exp\left(-\frac{\phi(x) e_0 (-z)}{k_B T} \right)}{\epsilon_0 \epsilon_r}. \tag{2.20}$$

if the mathematical identity $\sinh(x) = \frac{e^x - e^{-x}}{2}$ is used, it is possible to reduce Eq. 2.20 to

$$\frac{d^2\phi(x)}{dx^2} = \frac{2 n^0 z e_0}{\epsilon_0 \epsilon_r} \sinh\left(\frac{\phi(x) e_0 z}{k_B T} \right). \tag{2.21}$$

Multiplying both sides of Eq. 2.21 by $2\frac{d\phi(x)}{dx}$ yields

$$2\frac{d\phi(x)}{dx}\frac{d^2\phi(x)}{dx^2} = \frac{2n^0 ze_0}{\epsilon_0\epsilon_r}\sinh\left(\frac{\phi(x)e_0 z}{k_B T}\right)2\frac{d\phi(x)}{dx}, \tag{2.22}$$

or

$$\frac{d}{dx}\left(\frac{d\phi(x)}{dx}\right)^2 = \frac{4n^0 ze_0}{\epsilon_0\epsilon_r}\sinh\left(\frac{\phi(x)e_0 z}{k_B T}\right)\frac{d\phi(x)}{dx} \tag{2.23}$$

Integrating Eq. 2.23

$$\int_\infty^{x'} d\left(\frac{d\phi(x)}{dx}\right)^2 = \int_\infty^{x'} \frac{4n^0 ze_0}{\epsilon_0\epsilon_r}\sinh\left(\frac{\phi(x)e_0 z}{k_B T}\right)d\phi(x), \tag{2.24}$$

yields

$$\left(\frac{d\phi(x)}{dx}\right)^2 = \frac{4n^0 k_B T}{\epsilon_0\epsilon_r}\left(\cosh\left(\frac{\phi(x)e_0 z}{k_B T}\right) - 1\right). \tag{2.25}$$

The first term was obtained using the boundary condition $\phi'_\infty = lim_{x\to\infty}\frac{d\phi(x)}{dx} = 0$ in

$$\int_\infty^{x'} d\left(\frac{d\phi(x)}{dx}\right)^2 = \left(\frac{d\phi(x)}{dx}\right)^2\Bigg|_\infty^{x'} = \left(\frac{d\phi(x')}{dx'}\right)^2, \tag{2.26}$$

while the second term of 2.25 was calculated using $\int \sinh(ax) = \frac{1}{a}\cosh(ax) + C$

and the boundary condition $\phi_\infty = lim_{x\to\infty}\phi(x) = 0$ in

$$\int_\infty^{x'} \frac{4n^0 ze_0}{\epsilon_0\epsilon_r}\sinh\left(\frac{\phi(x)e_0 z}{k_B T}\right)d\phi(x) = \frac{4n^0 ze_0}{\epsilon_0\epsilon_r}\frac{k_B T}{e_0 z}\cosh\left(\frac{\phi(x)e_0 z}{k_B T}\right)\Bigg|_\infty^{x'}, \tag{2.27}$$

which reduces to

$$\int_\infty^{x'} \frac{4n^0 ze_0}{\epsilon_0\epsilon_r}\sinh\left(\frac{\phi(x)e_0 z}{k_B T}\right)d\phi(x) = \frac{4n^0 k_B T}{\epsilon_0\epsilon_r}\left(\cosh\left(\frac{\phi(x')e_0 z}{k_B T}\right) - 1\right). \tag{2.28}$$

If this mathematical identity $\cosh(x) - 1 = 2\sinh^2(\frac{x}{2})$ is used in Equation 2.25, it is possible to obtains:

$$\left(\frac{d\phi(x)}{dx}\right)^2 = \frac{8n^0 k_B t}{\epsilon_0 \epsilon_r} \sinh^2\left(\frac{\phi(x)\epsilon_0 z}{2k_B t}\right). \tag{2.29}$$

Eq.2.29 can be also written as

$$\frac{d\phi(x)}{dx} = -\sqrt{\frac{8n^0 k_B t}{\epsilon_0 \epsilon_r}} \sinh\left(\frac{\phi(x)\epsilon_0 z}{2k_B t}\right). \tag{2.30}$$

Notice that the function $\sinh(x) = \frac{e^x - e^- x}{2}$ is positive for $x > 0$, and negative for $x < 0$. The negative sign in 2.30 implies that positive values of the mean electrostatic potential, $\phi(x) > 0$, have associated a negative slope, $\frac{d\phi(x)}{dx} < 0$, while for $\phi(x) < 0$ the slope of the mean electrostatic potential is positive $\frac{d\phi(x)}{dx} > 0$. This allows to satisfy the condition $\phi_\infty = lim_{x\to\infty}\phi(x) = 0$ in the bulk electrolyte.

The Debye k_D-parameter for a $z:z$ electrolyte can written as

$$k_D = \sqrt{\frac{e^2 \sum_{i=1}^{2} n_i^0 z_i^2}{\epsilon_0 \epsilon_r k_B T}} = \sqrt{\frac{2e_0^2 n^0 z^2}{\epsilon_0 \epsilon_r k_B T}}. \tag{2.31}$$

If we multiply k_D by $\frac{2k_B T}{z e_0}$, we obtain

$$\frac{2k_B T}{ze} k_D = \sqrt{\frac{4k_B^2 T^2}{z^2 e_0^2}} \sqrt{\frac{2e_0^2 n^0 z^2}{\epsilon_0 \epsilon_r k_B T}} = \sqrt{\frac{8n^0 k_B T}{\epsilon_0 \epsilon_r}}. \tag{2.32}$$

Substituting Eq. 2.32 in Eq.2.30 yields

$$\frac{d\phi(x)}{dx} = -\frac{2k_B T}{z e_o} k_D \sinh\left(\frac{\phi(x) e_o z}{2k_B T}\right). \tag{2.33}$$

Let us consider the change of variables $\psi(x) = \frac{e_0 z}{2k_B T}\phi(x)$ in Eq. 2.33 to obtain

$$\frac{d\psi(x)}{dx} = -k_D \sinh(\psi(x)), \tag{2.34}$$

which can be re-written as

$$\frac{d\psi(x)}{\sinh(\psi(x))} = -k_D dx. \tag{2.35}$$

Considering that $\int \frac{dx}{\sinh(x)} = ln(\tanh(\frac{x}{2})) + lnC$, Eq.2.33 can be integrated to yield

$$ln\left(\tanh\left(\frac{\psi(x)}{2}\right)\right) + lnC = -k_D x. \tag{2.36}$$

The integration constant can be easily found considering that at the closest approach position of ions, $x = x_0$, the mean electrostatic potential is $\psi_0 = \psi(x_0)$:

$$lnC = -k_D x_0 - ln\left(\tanh\left(\frac{\psi_0}{2}\right)\right). \tag{2.37}$$

Replacing Eq. 2.37 in Eq. 2.36 produces

$$ln\left(\tanh\left(\frac{\psi(x)}{2}\right)\right) - k_D x_0 - ln\left(\tanh\left(\frac{\psi_0}{2}\right)\right) = -k_D x, \tag{2.38}$$

which can be recast as

$$ln\left(\frac{\tanh\frac{\psi(x)}{2}}{\tanh\frac{\psi_0}{2}}\right) = -k_D x + k_D x_0, \tag{2.39}$$

to obtain finally the mean electrostatic potential as a function of the distance:

$$\tanh\left(\frac{\psi(x)}{2}\right) = \tanh\left(\frac{\psi_0}{2}\right) exp(-k_D(x - x_0)), \tag{2.40}$$

or

$$\tanh\left(\frac{e_0 z\phi(x)}{4k_B T}\right) = \tanh\left(\frac{e_0 z\phi_0}{4k_B T}\right) exp(-k_D(x - x_0)). \tag{2.41}$$

Surface charge density, integral and differential capacities

The surface charge density of the ionic cloud (total charge per area unit) is given by:

$$\sigma_0' = \int_{x_0}^{\infty} \rho(x)dx = -\frac{4n^0 e_0 z}{k_D} \sinh\left(\frac{\phi(x)e_0 z}{2k_B T}\right). \tag{2.42}$$

Let us define σ_0 as the surface charge density of the charged plate. Using the electroneutrality condition $\sigma_0 = -\sigma_0'$ it is found that

$$\sigma_0 = \frac{4n^0 e_0 z}{k_D} \sinh\left(\frac{\phi_0 e_0 z}{2k_B T}\right). \tag{2.43}$$

For $\frac{\phi(x)e_0 z}{2k_B T} < 1$ it is possible approximate $\sinh(x) \approx x$ and hence

$$\sigma_0 = \frac{4n^0 e_0 z}{k_D}\left(\frac{\phi_0 e_0 z}{2k_B T}\right) = \frac{2n^0 e_0^2 z^2}{\epsilon_0 \epsilon_r K_B T}\frac{\epsilon_0 \epsilon_r}{k_D} \tag{2.44}$$

which can be simplified as

$$\sigma_0 = \epsilon_0 \epsilon_r k_D \phi_0. \tag{2.45}$$

Let us define the ratio between the surface charge density at the charged plate, σ_0, and the mean electrostatic potential, ϕ_0, as the integral capacitance per area unit $K_0 = \frac{\sigma_0}{\phi_0}$. In the linearized Poisson-Boltzmann (Debye-Hückel) theory the integral capacitance is proportional to the k_D-parameter:

$$K_0 = \frac{\sigma_0}{\phi_0} = \epsilon_0 \epsilon_r k_D. \tag{2.46}$$

Physically, this result is analogous to the capacity of a charged plates capacitor, with a surface charge density σ_0 and $-\sigma_0$ in each plate, separated by a distance $\frac{1}{k_D}$ at a difference of electrostatic potential ϕ_0. It is also possible to define the differential capacity as $C_0 = \frac{d\sigma_0}{d\phi_0}$. In the Debye-Hückel approximation the integer and differential capacities are the same:

$$C_0 = K_0 = \frac{d\sigma_0}{d\phi_0} = \epsilon_0 \epsilon_r k_D. \tag{2.47}$$

In the non-linear Poisson-Boltzmann theory, the differential capacity can be obtained from Eq. 2.43:

$$C_0 = \frac{d\sigma_0}{d\phi_0} = \frac{2n^0 e_0^2 z^2}{k_D k_B T} \cosh\left(\frac{\phi_0 e_0 z}{2k_B T}\right). \tag{2.48}$$

2.2 The linearized Poisson-Boltzmann theory in spherical geometry

The Poisson equation in spherical coordinates can be written as

$$\nabla^2\phi(r) = \frac{1}{r^2}\frac{d}{dr}\left(r^2\frac{d\phi}{dr}\right) = -\frac{\rho(r)}{\epsilon_0\epsilon_r}. \tag{2.49}$$

Let us consider a charged sphere of radius a_0 surrounded by ions, which have a closest approach distance $x_0 = a_0 + d$ (see Figure 2.2). As it was done in the planar geometry, substituting Eq 2.9. in Eq. 2.49 for a binary $z:z$ electrolyte yields

$$\nabla^2\phi(r) = -\frac{\sum_{i=1}^{m} n_i^0 z_i e_0 exp\left(-\frac{\phi(x)e_0 z_i}{k_B T}\right)}{\epsilon_0\epsilon_r}, \tag{2.50}$$

which can be also written as

$$\nabla^2\phi(r) = -\frac{2n^0 z e_0}{\epsilon_0\epsilon_r}\sinh\left(\frac{\phi(x)e_0 z}{k_B T}\right). \tag{2.51}$$

Using the definition of the Debye k_D-parameter for a $z:z$ electrolyte given in Eq. 2.31, and using the change of variable $\psi(r) = \frac{e_\phi(x)}{k_B T}$, it is possible to recast Eq. 2.51 as

$$\nabla^2\psi(r) = \frac{k_D^2}{z}\sinh(z\psi(r)). \tag{2.52}$$

For $\psi(r) < 1, \sinh(x) \approx x$ and Eq. 2.52 can be linearized:

$$\nabla^2\psi(r) = k_D^2\psi(r), \tag{2.53}$$

or

$$\nabla^2\phi(r) = k_D^2\phi(r). \tag{2.54}$$

The solution of Eq. 2.54 is of the form:

$$\phi(r) = constant \times \frac{x_0}{r} exp(-k_D(r - x_0)). \tag{2.55}$$

The charge of the diffuse electrical double layer, Q_0', is given by

$$Q_0' = \int_{x_0}^{\infty} 4\pi r^2\rho(r)dr = -4\pi\epsilon_0\epsilon_r\phi_0 x_0(1 + k_D x_0), \tag{2.56}$$

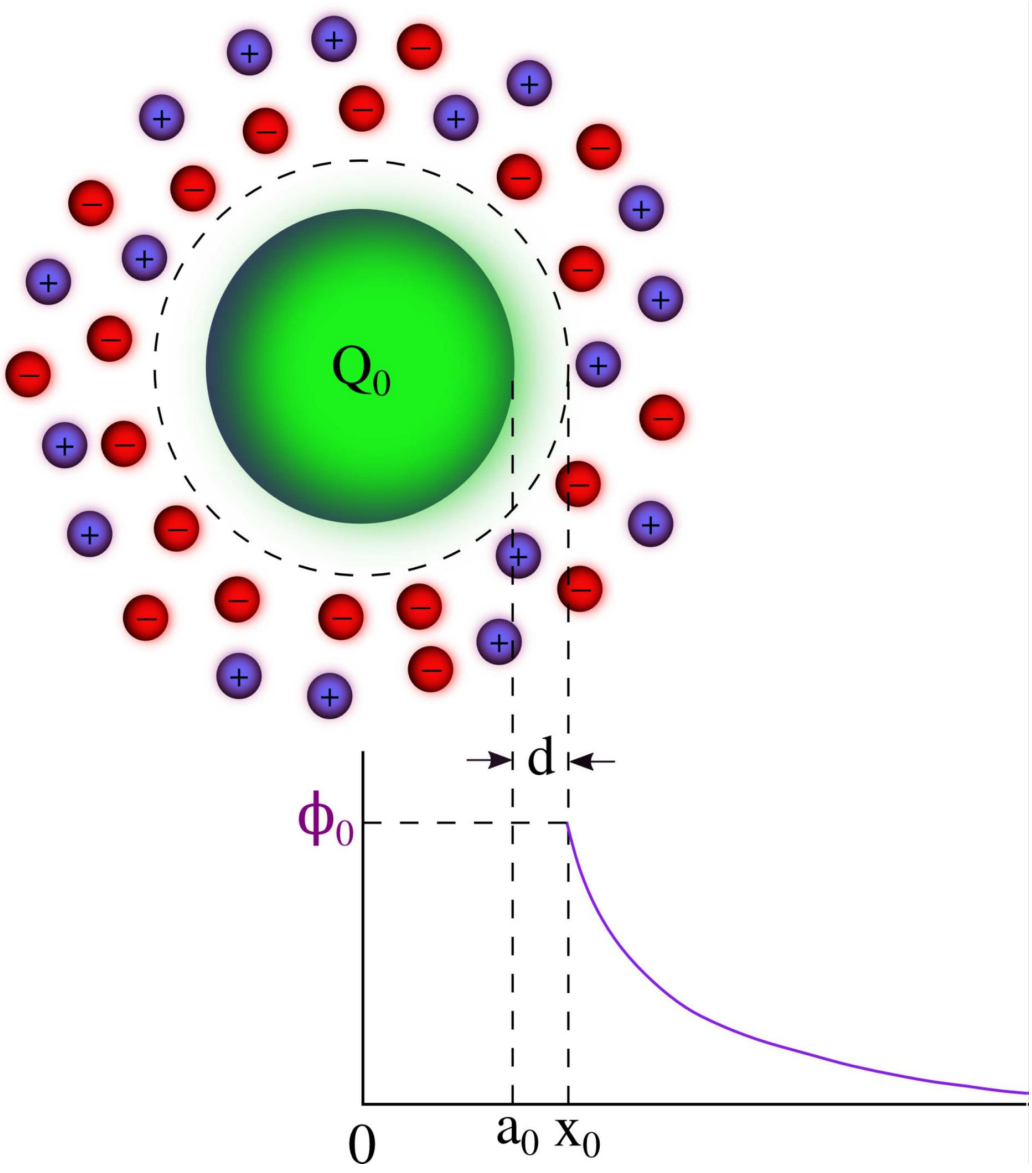

Figure 2.2: Schematic representation of the diffuse electrical double layer in spherical geometry.

Using the electroneutrality condition $Q_0 + Q_0' = 0$, where Q_0 is the charge of the nanoparticle, it is possible to write the mean electrostatic potential at $x = x_0$ using Eq. 2.56 as

$$\phi_0 = \frac{Q_0}{4\pi\epsilon_0\epsilon_r x_0(1 + k_D x_0)}. \tag{2.57}$$

Substituting Eq. 2.57 in Eq. 2.55 gives:

$$\phi(r) = \frac{1}{4\pi\epsilon_0\epsilon_r}\frac{Q_0}{1 + k_D x_0}\frac{exp(-k_D(r - x_0))}{r}, \tag{2.58}$$

which is the mean electrostatic potential as a function of the distance in the linearized Poisson-Boltzmann theory.

It is straightforward to show that Eq. 2.57 can be written as:

$$\phi_0 = \frac{Q_0}{4\pi\epsilon_0\epsilon_r x_0} + \frac{-Q_0}{4\pi\epsilon_0\epsilon_r(x_0 + \frac{1}{k_D})}. \tag{2.59}$$

Physically, this means that the difference of the mean electrostatic potential in the spherical electrical double layer can be viewed as that produced by a spherical capacitor.

2.3 The Poisson-Boltzmann integral equation

The representation of the electrical double layer used in this thesis is based on the well-known restricted primitive model of a binary electrolyte. In this description, a colloid is represented by a hard and uniformly charged sphere of radius R_M and surface charge density ($\sigma_0 = Q_M/4\pi R_M^2$), where $Q_M = Z_M e_0$ is the colloidal charge, Z_M is the valence of the colloid, and e is the protonic charge. The spherical macroion is surrounded by an equally-sized z:1 electrolyte, asymmetric in valence, with monovalent counterions and multivalent coions. Ions are represented by hard spheres of diameter a with point charges $q_i = z_i e$ embedded at their centers, such that z_i is the valence of the ionic species i. The spherical macroion and all ions are immersed in a continuum aqueous solvent characterized by a dielectric constant $\epsilon = 78.5$ at a temperature T = 298 K in all instances.

The pair interaction potential between any pair of charged particles in spherical geometry, used in the integral equation theory, is given by:

$$U_{ij}(r) = \begin{cases} \infty, r < r_i + r_j \\ \frac{z_i z_j e_0^2}{4\pi\epsilon_0\epsilon_r}, r \geq r_i + r_j \end{cases} \tag{2.60}$$

where the subscripts $i, j = M$, +, -; and r denotes the distance between the centers of two charged particles of types i and j with radii r_i and r_j, respectively.

The closest approach distance between the ions of diameter a and the macroion of radius R_M is the so-called Helmholtz plane $r_H = R_M + (a/2)$ (see Figure 2.3).

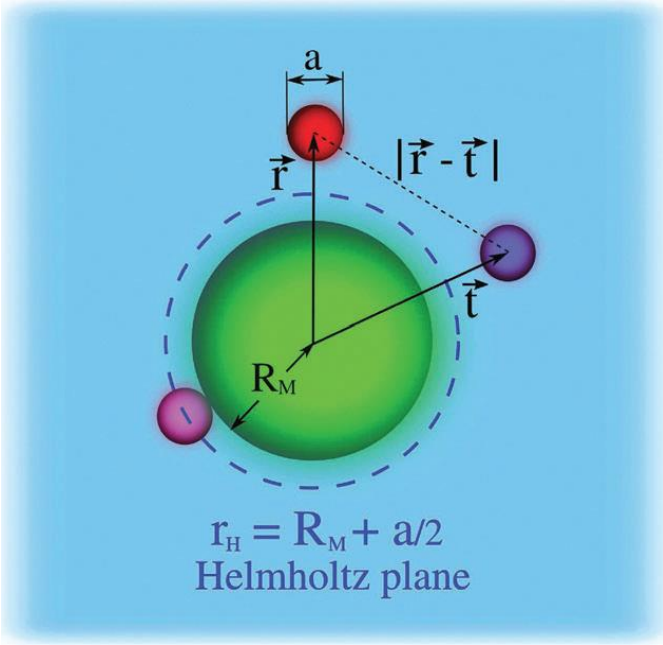

Figure 2.3: Schematic representation of the model system.

The integral equation description is obtained by solving numerically the Ornstein–Zernike equations using approximate closures. The Ornstein–Zernike equations describing the ionic cloud around a single macroion can be written as

$$h_{Mj}(r) = C_{Mj}(r) + \sum_{k=-,+} \rho_k \int h_{Mk}(t) c_{kj}(\left|\vec{r} - \vec{t}\right|) dV, for\, j = -, + \tag{2.61}$$

where $h_{Mj}(r) = g_{Mj}(r) - 1$ are the total ionic correlation functions, and $g_{Mj}(r)$ are the ionic radial distribution functions. Here, the direct correlation functions between ions and the spherical colloid are specified using the hypernetted-chain (HNC) closure $c_{Mj}(r) = -\beta U_{Mj}(r) + h_{Mj}(r) - ln[h_{Mj}(r) + 1]$. If ion-ion direct correlation functions are approximated by the ionic electrostatic energy $c_{kj}(\left|\vec{r} - \vec{t}\right|) = (z_k z_j e^2)/(4\pi\epsilon_0\epsilon \left|\vec{r} - \vec{t}\right|)$ the integral equation version of the non-linear

Poisson–Boltzmann theory is obtained.

From the ionic profiles obtained from the non-linear Poisson–Boltzmann theory it is possible to calculate several thermodynamic and electrical properties of the charged particles in solution. Specifically, the integrated charge, the electric field, and the mean electrostatic potential around a spherical macroion can be written, respectively, as

$$P(r) = z_M + \sum_{k=-,+} \int_0^r z_i \rho_i g_i(t) 4^2 \, dt, \tag{2.62}$$

$$E(r) = \frac{e_0}{4\pi\epsilon_0\epsilon} \frac{P(r)}{r^2}, \tag{2.63}$$

and

$$\Psi(r) = -\int_\infty^r E(t)dt = \int_r^\infty E(t)dt. \tag{2.64}$$

Physically, the integrated charge is the net charge (in units of e_0) enclosed in a sphere of radius r centered in the macroion, and is a measure of the neutralization capacity of the surrounding electrolyte. The electric field is proportional to the electrostatic component of the mean force that a charged particle experience due to its coulombic interaction with the colloidal particle and the ions of the electrolyte. The mean electrostatic potential quantifies the electrostatic screening of the bare colloidal charge by the electrolyte. The mean electrostatic potential evaluated close to the Helmholtz plane has been conventionally associated with the so-called zeta potential, ζ. This last quantity is usually defined as the mean electrostatic potential at the slipping plane in electrokinetic phenomena.

2.4 The O'Brien and White theory of electrophoresis

Consider a single and charged spherical colloid, of radius R and surface charge density σ_0, immersed in a point-ions binary electrolyte. In addition, the solvent is considered a continuous medium and all the system has a uniform dielectric constant, ϵ, and is at a temperature T. If an external electrical field, $\vec{E}_0$, is applied, the colloid experiences a drift which, after some transient, takes a constant value $\vec{U}_0$, that we will name as the electrophoretic velocity of the macroparticle. For simplicity, from now on, we will describe the dynamics in terms of coordinate axes whose origin coincides with the center of the sphere. If the electrolyte behaves as a newtonian fluid of dynamic viscosity η and the asssociated Reynolds number is small, the governing equations of the system are (*10*):

$$\eta\nabla^2\vec{u}(\vec{r}) - \nabla p(\vec{r}) = \rho_c(\vec{r})\nabla\psi(\vec{r}), \tag{2.65}$$

where $\vec{u}(\vec{r})$, $p(\vec{r})$, $\rho_c(\vec{r})$, and $\psi(\vec{r})$ are, respectively, the velocity, pressure, volumetric charge density, and electrostatic potential at a distance $\vec{r}$ of the origin. In particular, $\rho_c(\vec{r}) = \sum_i ez_i\rho_i(\vec{r})$, such that e is the *protonic* charge, and z_i and $\rho_i(\vec{r})$ are the valence and volumetric number density of the electrolytic species i. Note that

$$\rho_i(\vec{r}) = \rho_i g_i(\vec{r}), \tag{2.66}$$

with ρ_i and $g_i(\vec{r})$ being the bulk density and the distribution function of each ionic component.

Since the electrolyte is an incompressible fluid

$$\nabla \cdot \vec{u}(\vec{r}) = 0. \tag{2.67}$$

On the other hand, the electrostatic potential fulfills the Poisson equation

$$\nabla^2\psi(\vec{r}) = -\frac{1}{\epsilon_0\epsilon_r}\rho_c(\vec{r}). \tag{2.68}$$

Complementary, the ionic species follow the equations

$$\nabla \cdot (\rho_i(\vec{r})\,\vec{v}_i(\vec{r})) = 0 \tag{2.69}$$

and

$$-\lambda_i(\vec{v}_i(\vec{r}) - \vec{u}(\vec{r})) - ez_i\nabla\psi(\vec{r}) - k_BT\nabla\ln\rho_i(\vec{r}) = \vec{0}, \tag{2.70}$$

where λ_i is the ionic drag coefficient and k_B is the Boltzmann constant. The pair of preceding equations can be combined as

$$\nabla \cdot (k_BT\nabla\rho_i(\vec{r}) + ez_i\rho_i(\vec{r})\nabla\psi(\vec{r}) - \lambda_i\rho_i(\vec{r})\vec{u}(\vec{r})) = 0. \tag{2.71}$$

The corresponding boundary conditions are:

$$\vec{u}(R) = 0, \tag{2.72}$$

$$\vec{u}(\infty) = -U_0\,\hat{e}_x, \tag{2.73}$$

$$\psi(R) = \zeta, \tag{2.74}$$

$$-\nabla\psi(\infty) = E_0\,\hat{e}_x, \tag{2.75}$$

$$\rho_i(\infty) = \rho_i \tag{2.76}$$

and

$$\vec{v_i}(R)\cdot\hat{n} = 0, \tag{2.77}$$

or else,

$$(ez_i\nabla\psi(R) + k_BT\nabla\ln\rho_i(R))\cdot\hat{n} = 0. \tag{2.78}$$

It must be noted that, in the above equations, all the variables are stationary non-equilibrium quantities. Thus, to proceed to the numerical solution of this set of non-linear partial differential equations, we express any variable, $A(\vec{r})$, in the general perturbative form:

$$A(\vec{r}) = A^{eq}(r) + \delta A(\vec{r}), \tag{2.79}$$

with $A^{eq}(r)$ being the value *at equilibrium* of $A(\vec{r})$. Inserting those perturbation forms in the governing equations and keeping the first-order terms, we arrive to the following system for the δA functions:

$$\nabla^2\delta\psi(\vec{r}) = -\frac{1}{\epsilon_0\epsilon_r}\delta\rho_c(\vec{r}), \tag{2.80}$$

$$\eta\nabla^2\vec{u}(\vec{r}) - \nabla p(\vec{r}) = \rho_c^{eq}(r)\nabla\delta\psi(\vec{r}) + \delta\rho_c(\vec{r})\nabla\psi^{eq}(r) \tag{2.81}$$

and

$$\nabla\cdot(k_BT\nabla\delta\rho_i(\vec{r}) + ez_i\rho_i^{eq}(r)\nabla\delta\psi(\vec{r}) + ez_i\delta\rho_i(\vec{r})\nabla\psi^{eq}(r) - \lambda_i\rho_i^{eq}(r)\vec{u}(\vec{r})) = 0, \tag{2.82}$$

such that

$$\delta\rho_c(\vec{r}) = \sum_i ez_i\delta\rho_i(\vec{r}). \tag{2.83}$$

We must emphasize that the determination of the perturbation (i.e., *non-equilibrium*) unknowns $\delta A(\vec{r})$ assumes the prior knowledge of the quantities A at *equilibrium*. In particular, in the classical description by O'Brien and White

$$\vec{u}^{eq}(r) = \vec{0}, \tag{2.84}$$

by definition of equilibrium, and

$$\psi^{eq}(r) = \psi^{PB}(r). \tag{2.85}$$

In the previous equation, $\psi^{PB}(r)$ is the electrostatic potential that accomplishes the Poisson-Boltzmann equation, i.e.,

$$\psi^{PB}(r) = -\frac{k_BT}{ez_i}\ln g_i(r), \tag{2.86}$$

where $g_i(r)$, for $i = -,+$, are the solutions to the pair of Poisson-Boltzmann integral equations, discussed in Section 2.3.

Finally, and following the clever mathematical procedure devised by O'Brien and White (*10*), the previous system of can be recast as a set of *ordinary* differential equations that can be solved via any usual numerical technique.

Once the numerical determination of all the functions δA is completed, the value of the colloidal electrophoretic mobility, μ, is given by

$$\mu = \frac{U_0}{E_0}. \tag{2.87}$$

Specifically, to obtain μ in this thesis we have used a Fortran code, developed by González-Tovar (*11*, *12*), that solves numerically the O'Brien and White theory via a robust combination of the Finite Element and Runge-Kutta methods.

CHAPTER 3

An experimental set up for microscopic colloids characterization

In the present chapter we described the setup developed to measure colloidal electrophoretic mobilities at the University of Sinaloa.

In the year 2003 the Faculty of Physics and Mathematics of the Universidad Autónoma de Sinaloa acquired an equipment for electrophoretic mobility measurements, the Zetameter 3.0. In the year 2005 the equipment was packaged and stored and, afterwards, was not used anymore.

In the present work we describe the process to refurbish the equipment with the purpose of implement an experimental colloids laboratory. The stored equipment was aged, some parts did not work properly and other did not work at all. We restored and also carried out the process of maintaining the measurement cell and the optical and video components attached.

3.1 Experimental set up

The experimental setup used for electrophoretic mobility measurements is shown in Figure 3.1. The entire arrangement consists of:

Figure 3.1: Zeta meter equipment used in the present work to measure electrophoretic mobility of SiO_2 and PS microparticles.

- Electrophoretic cell (Type GT-2 cell, see Figure 3.2 (a)). It holds the sample for viewing under the microscope. It consists of two electrode chambers connected by an optically polished electrophoresis tube (10 cm long and 4 cm diameter) The cell body consists of two Polytetrafluoroethylene (Teflon) sections with a fused quartz section in the center. Each Teflon section contains a portion of the cell tube and an electrode chamber. The quartz centre section is for analyzing the colloidal suspensions using the microscope.

- Electrodes. Each cell requires two electrodes, an anode and cathode. We used a Molybdenum cylinder anode (see Figure 3.2 (b)). This electrode was designed to combine with gaseous oxygen as it evolves from the anode, preventing false colloids migration (due to gas production). It can be used with all samples, however, it turns from a metallic color to blue-black or black due to an oxide layer created during the its prolonged use. The Cathode that we used is a Platinum rod cathode. Platinum material can be used for any systems without any specific conductance limitation. The oxide layer is not created using this material. It is possible to acquired a platinum Rod anode, but it is too expensive.

- Display unit. The data display shows several parameters such as: number of colloids that have been tracked, their average zeta potential (or electrophoretic mobility) and the statistical standard deviation of the values measured (see Figure 3.2 (c)). Also, temperature and average specific conductance can be measured, then they are reported in the display unit. It consists of:

  i. A Power On/Off Switch

  ii. Microscope Module Control. The light intensity can be varied to improve the microscope illumination (by varying the brightness)

  iii. Output Jacks. They receive the plugs attached to the electrode leads.

  iv. Function switch. This switch controls the power supply and the options that it controls are:

    (a) Stand by: Send the DC voltage applied to the output jacks to zero.

    (b) Energize electrodes: Energize the electrodes to the voltage selected (V).

    (c) Specific conductance: Energize the output jacks to measure the specific conductance of the sample ($\mu S/cm$).

    (d) K factor test: This reads the K factor used to measure the specific conductance of the electrophoresis cell. This can be varied depending on the cell used.

  v. Voltage setting switch. Using this switch, the DC voltage applied can be selected (from 20 to 300V).

  vi. Display units switch. The display can show the results of the measures in time (s), electrophoretic mobility ($\mu m/s$ per V/cm) and zeta potential (mV) units.

vii. Ocular micrometer switch. The microscope eyepiece has three different tracking distances (they are printed into the ocular micrometer), full, quarter and eight scale. This scale is chosen depending on the colloid velocity.

viii. Keypad. This is used as a joystick to select the particles movement.

- Microscope module. The microscope module used in this work is shown in Figure 3.2 (c). Is a Unitron FSB-4x microscope with standard objectives 4x, Standard eyepieces 20x and magnifications 80x. To make particle tracking, a CCD is coupled to the microscope (HITACHI KP-M2U) and the images in real time are observed using a video monitor (HITACHI VM-122OU). In figure 3.2 (d) an image of a calibration experiment (Silica particles) is shown.

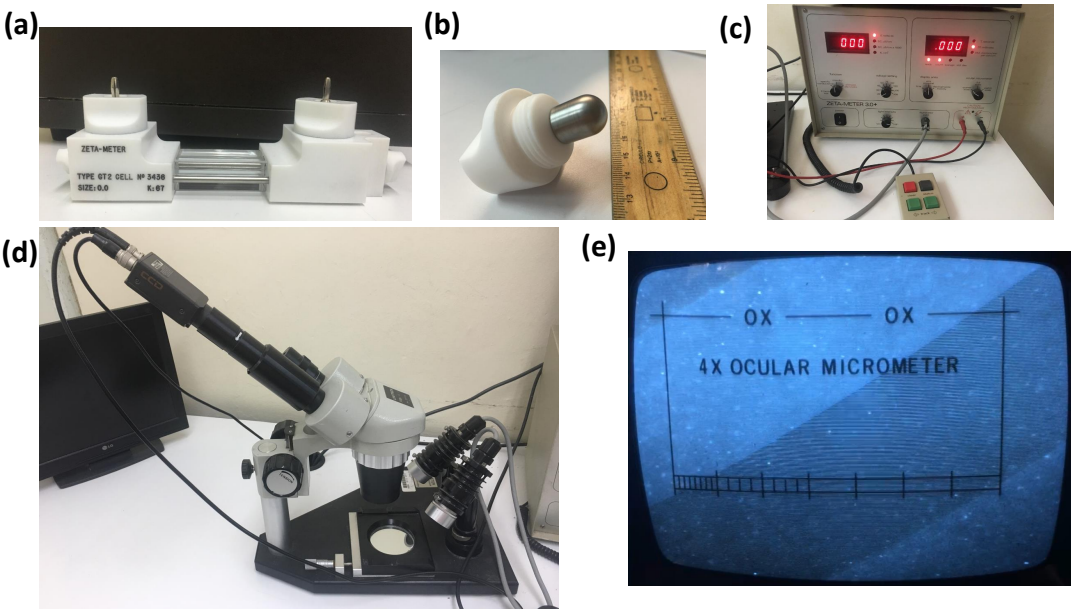

Figure 3.2: The different components of the Zeta meter equipment. a) Electrophoretic cell. b) Molibdene electrode. c) Display unit. d) Microscope module. e) Video monitor.

The electrophorectic mobility measurements are direct and manual. The electrophoresis cell is filled with the sample ($\approx 20ml$), then an electric field is applied and the colloidal particles start to migrate from anode to cathode or from cathode to anode (this direction indicates if their electrical charge is positive or negative). The colloids velocity is proportional to their electrophoretic mobility (see Section 2).

The colloids movement is observed and tracked with the CCD coupled to the microscope (Figure 3.2). First a particle is selected, then using the joystick it is tracked, when the particle crosses the reticle with the scale selected, the joystick is pressed and then it is released as the

particle crosses the end of the scale in the grid. We tracked twenty particles and then the sample was change. Three samples were measured for each experiment varying salt concentration and salts type to analyze.

3.2 Experimental samples

The particles used in this work were: Silica ($SiO_2 1.16\mu m$) and Polystyrene (PS $1.6\mu m$). The particle concentration was fixed at $\Phi_m = 0.0005\%$. The salts used in this study were: NaCl and $CaCl_2$. To study the role of the ionic strength in the particle electrophoretic mobilities, the salt concentration was varied from 1mM to 500mM (in the case of NaCl).

To study only the role of the variation in the ionic strength due to the salt concentration and not due to variations in the pH of the particle suspension, the salts were diluted in buffer solution of low ionic strength at pH7. A buffer solution is an aqueous solution consisting of a mixture of a weak acid and its conjugate base or a weak base and its conjugate acid. This composition enables the stabilization of the medium pH. The chemical compound used in the preparation of pH7 buffer solution was NaH_2PO_4. In order to obtain the precise pH value, a small amount of $NaOH$ was added. The contribution to the ionic strength was negligible $\approx 1.13mM$

3.3 Zeta-meter Calibration

To calibrate the zeta meter equipment, we used Min-U-Sil particles, which are an inexpensive silica particles produced by crushing sandstone. The particle diameter is $\approx 1.6.\mu M$. In table 3.1 some chemical characteristics are presented.

	(%)
SiO_2 (Silicon Dioxide)	99.4
Fe_2O_3(Iron Oxide)	0.031
Al_2O_3 (Aluminum Oxide)	0.26
TiO_2 (Titanium Dioxide)	0.01

Tabla 3.1: Typical Chemical Analysis of Min-U-Sil particles, %.

To prepare the calibration solution we prepared a suspension of 100mg/l of Min-U-Sil particles and 10gr of NaCl. First we prepared a stock suspension by adding 10gr of Min-U-Sil and 10gr of NaCl in one liter of distilled water. Then we prepared the test suspensions by adding 10ml of the stock suspension to one liter of distilled water. Finally we measure the Zeta Potential of the test suspension and the average will be about $-56 \pm 3mV$ with a standard deviation between 2 and

4.

3.4 Optimal concentration for mobility measurements

With the purpose of finding the optimal concentration of particle suspension for electrophoretic mobility measurements, we prepared particle suspensions with different concentration ranging from $\Phi_m = 1{\times}10^{-4}$ to 0.1%. The optimal concentration was found when particle electrophoretic mobility "saturated", regardless of the particle concentration. We used a concentration above this optimal value in order to assure that the electrophoretic mobility results obtained were not dependent of particle concentration. The results of particle electrophoretic mobility as a function of particle concentration are shown in Figure 3.3 for the Min U Sil particles diluted in buffer solution at pH7. This was repeated for the rest of particle suspensions. Finally, all the particle suspensions studied in the present work were diluted at a concentration of $\Phi_m = 0.0005\%$.

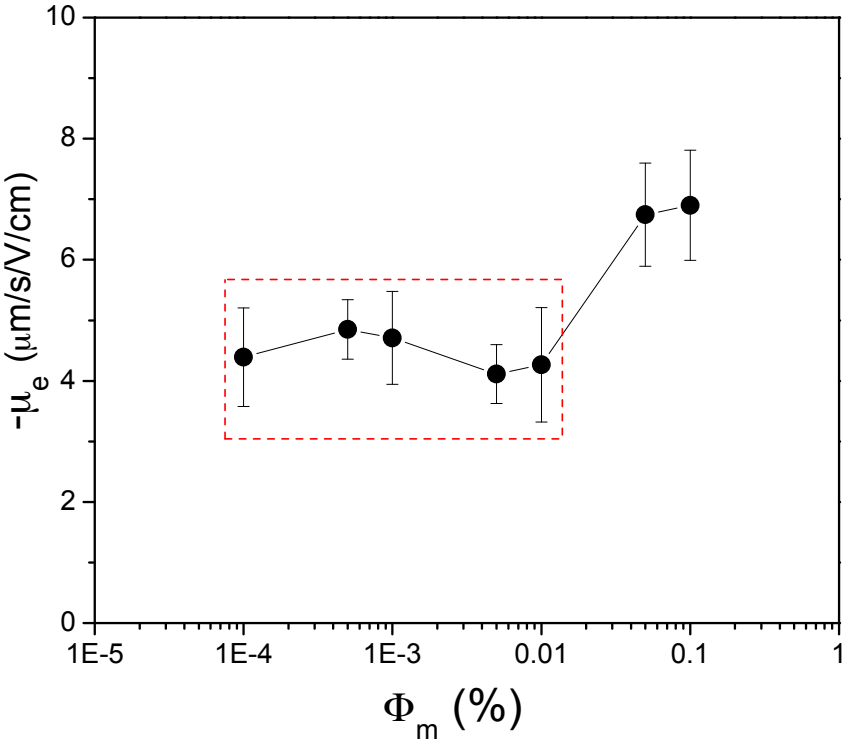

Figure 3.3: Electrophoretic mobility of Min-U-Sil particles as function of particle concentration. When the electrophoretic mobility saturated, we found the optimal concentration for electrophoretic mobility measurements.

CHAPTER 4

Results and discussion

In this chapter we present the results of electrophoretic mobility obtained using the Zeta meter equipment installed in the University of Sinaloa the Zetameter 3.0 described in Section 3. We also present the results obtained using the theoretical fitting developed by Dr. Enrique González Tovar and Dr. Ivan Guerrero García at the University of San Luis Potosí.

4.1 Experimental electrophoretic mobility

To compare the results obtained with our zeta meter, we measured electrophoretic mobilities using a Zetasizer of Brookhaven company. This device uses Phase Analysis Light Scattering (PALS). Firstly, a laser beam is used to illuminate the particles within the sample. Then, the incident laser beam passes through the sample and the scattered light is detected. When the electric field is applied to the suspension, the movement of the particles causes a fluctuation on the light intensity with a frequency proportional to the particle velocity due to the Doppler effect.

The experiments performed with our refurbished optical zetameter and the commercial light scattering zetameter were performed under the same conditions (same PS particles, particle concentration and temperature of the sample), which have been already described specifically in

Section 3.

In Figure 4.1 the results of the measurements of the electrophoretic mobility for PS microparticles obtained with both zetameters (Zetameter 3.0 and ZetaPALS) are presented. The electrolyte used for the experiment was NaCl (electrolyte 1:1). The concentration was varied from 0 to 0.5 M.

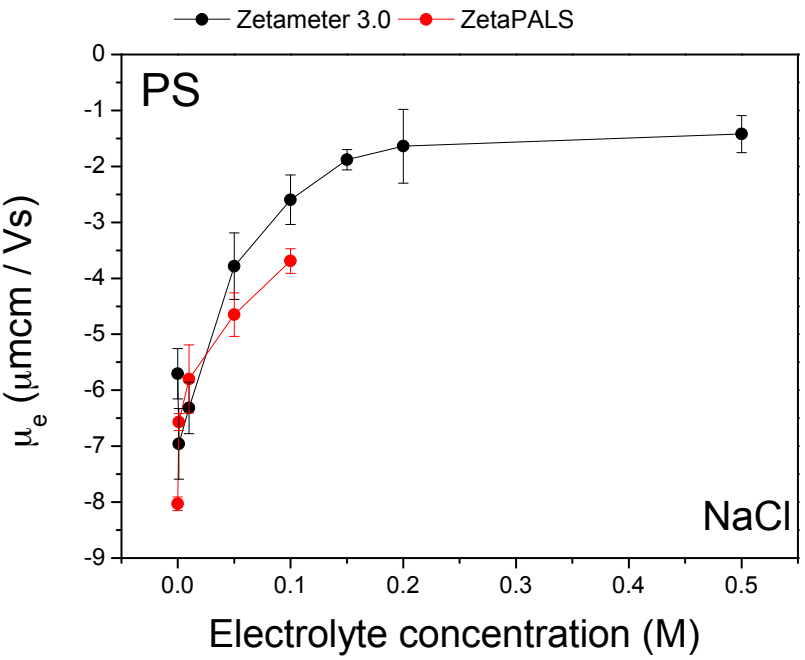

Figure 4.1: Comparison of electrophoretic mobility as function of NaCl concentration for PS microparticles using two different zetameters (Zetameter 3.0 and ZetaPALS).

In figure 4.2 we present the electroforetic mobility results associated to PS microparticles immersed in a 2:1 ($CaCl_2$) electrolyte. The electrolyte concentration was varied from 0 to 0.1 M.

A good agreement between the measurements performed with the two zetameters was obtained for the two electrolytes studied (NaCl and $CaCl_2$).

It is important to note that our optical zetameter allowed us to measure at higher electrolyte concentrations than the concentration allowed by the Zeta PALS equipment (see Figure 4.1 and 4.2). While the zetameter 3.0 allowed us to measure electrolyte concentration up to 0.5M (when NaCl was used) the Zeta PALS allowed us to measure up to a 0.1 M concentration of electrolyte.

For the $CaCl_2$ electrolyte the maximum electrolyte concentration measured was 0.1 M and 0.01 M for the Zetameter 3.0 and ZetaPALS respectively.

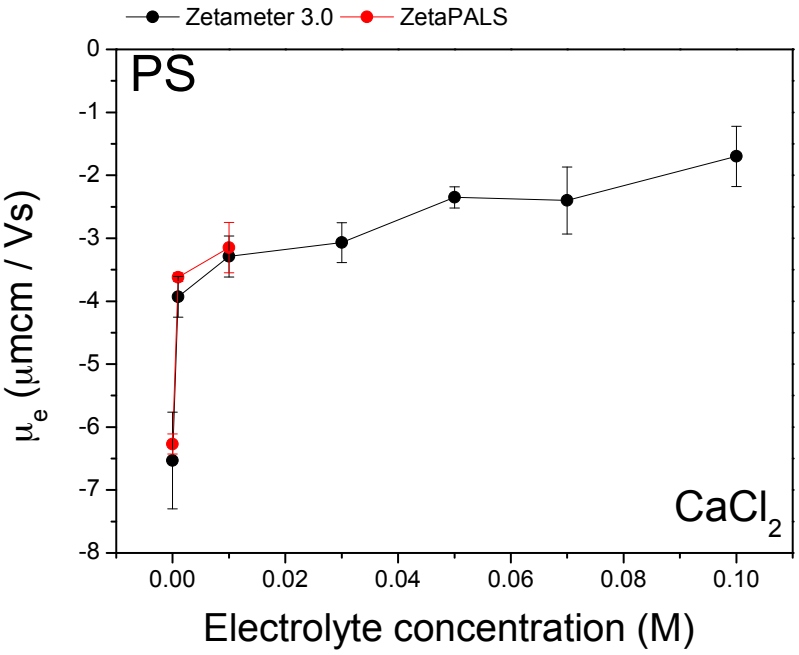

Figure 4.2: Electrophoretic mobility of PS microparticles as a function of the $CaCl_2$ concentration using two different zetameters (Zetameter 3.0 and ZetaPALS).

These results show that as the electrolyte concentration increases, the electrophoretic mobility reduces. As can be observed in Figure 4.1, the electrophoretic mobility reaches its minimum value at 0.15 M and after that it remains constant even if the electrolyte concentration further increases. On the other hand, we observed that at ionic concentrations higher than 0.5 M the PS microparticles started to aggregate. Thus, such experimental measurements were not considered.

The ionic strength is defined as:

$$I = -\frac{1}{2}\sum_{i=1}^{n} Z_i^2 C_i \tag{4.1}$$

where Z_i is the valence of the ions and C_i is the concentration of the dissolved ions. Notice that the magnitude of the electrophoretic mobility in the presence of divalent counterions ($CaCl_2$ electrolyte displayed in Figure 4.2) is lower than the electrophoretic mobility in the presence of monovalent counterions (NaCl electrolyte displayed in Figure 4.1) at the same salt concentration, and for all ionic concentrations measured. This is consistent with a higher ionic strength of 2:1 electrolytes regarding 1:1 salts at the same ionic concentration.

4.2 Theoretical Fitting

The theoretical fitting was performed in two parts. In the first part an equilibrium problem is solved. We supposed that the colloid is at equilibrium state and the fluid is moving. The ionic double layer of a binary electrolyte is generated around an electrical charged colloid using the non linear Poisson-Boltzmann theory.

We have considered 1:1 and 2:1 electrolytes, with an ionic diameter equal to 5 Å, surrounding a macroion with a diameter of 8000 Å.

In the second part, the electrophoretic mobility, including hydrodynamic effects due to the solvent, is calculated as a perturbation. The non-linear Poisson-Boltzmann theory in equilibrium is used as a reference system to calculate the stationary electrophoretic mobility according to a non-equilibrium theoretical scheme proposed by O'Brien and White.

4.2.1 Charge density calculation

In our experiments, we used different particles (see Section 3.2). Unfortunately we did not know the real particle charge density. Hence, to calculate it, we used a theoretical fitting. We calculated numerically the electrophoretic mobility for different charge densities when the electrolyte

concentration was fixed. This calculation was repeated until the numerical electrophoretic mobility matched the experimental mobility. The associated surface charge density is the electrokinetic charge of the macroion.

In Figures 4.3 and 4.4, the electrokinetic surface charge density calculated with the theoretical fitting is shown as a function of the ionic concentration for the 1:1 and 2:1 electrolytes, respectively.

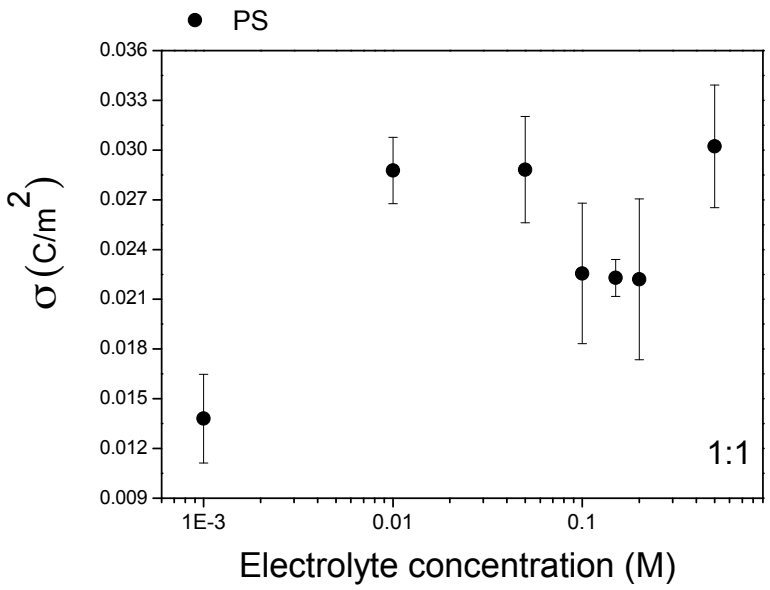

Figure 4.3: Charge density as function of electrolyte concentration for a electrolyte type 1:1 calculated using a theoretical fitting.

According to the Smoluchowski equation in the planar limit, the electrophoretic mobility is proportional to the zeta potential. If the ionic strength increases, the zeta potential decreases at a fixed colloidal charge in the Debye-Hückel approximation. Then, the behaviour observed experimentally in Figs. 4.1 and 4.2 is consistent with the Debye-Hückel approximation and the Smoluchowski equation in the planar limit for a constant bare colloidal charge. The use of the theoretical fitting allow us to estimate the electrokinetic charge associated to the electrophoretic mobilities measured experimentally. The most important feature observed in both Figs. 4.3 and 4.4 is the non-monotonic behaviour of the electrokinetic colloidal charge as a function of the ionic concentration.

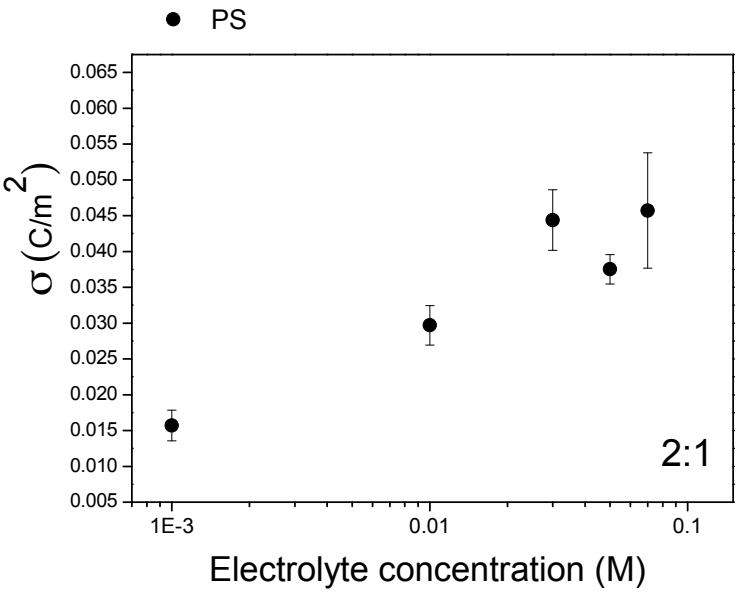

Figure 4.4: Charge density as function of electrolyte concentration for a electrolyte type 2:1 calculated using a theoretical fitting.

Another important property that can be estimated from the theoretical fitting is the mean electrostatic potential at the colloidal surface and at the Helmholtz plane. Conventionally, this last quantity is associated to the zeta potential. The zeta potential is one of the most important parameters characteristic of charged colloids in electrochemistry, and it is usually defined as the mean electrostatic potential at the shear plane of the colloid, when the charged colloidal particle moves due to the influence of an electric field.

4.2.2 Electrostatic potential calculation

Once we have found the electrokinetic charge associated to the experimental electrophoretic mobilities, as a function of the ionic concentration, we have calculated the mean electrostatic potential at the colloidal surface (represented by ψ_0) and the electrostatic potential at the Helmholtz plane (represented by Ψ_H) via the non-linear Poisson-Boltzmann theory . These quantities are shown in Figures 4.5 and 4.6 for the $1:1$ and $2:1$ electrolytes, respectively.

In both figures, we observe that Ψ_H decreases as a function of the electrolyte concentration. This trend is consistent qualitatively with the Smoluchowski equation in the planar limit assuming a constant bare colloidal charge. It is interesting to observe that the non-monotonic behaviour of the electrokinetic charge displayed in Figure 4.4, for a 2:1 electrolyte at high ionic concentrations, is strong enough to promote the non-monotonic behaviour of Ψ_0 in Figure 4.6.

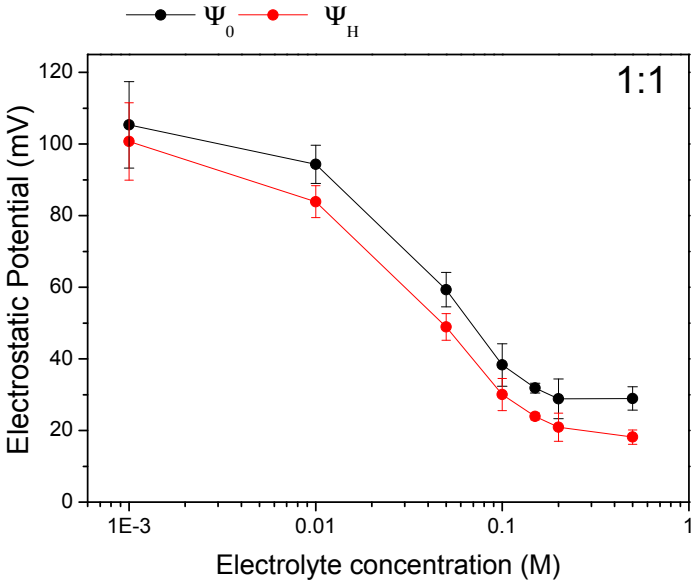

Figure 4.5: Plane Potential(Ψ_0) and Potential at the Helmholtz plane (Ψ_H) as function of electrolyte concentration for a electrolyte 1:1 calculated using a theoretical fitting.

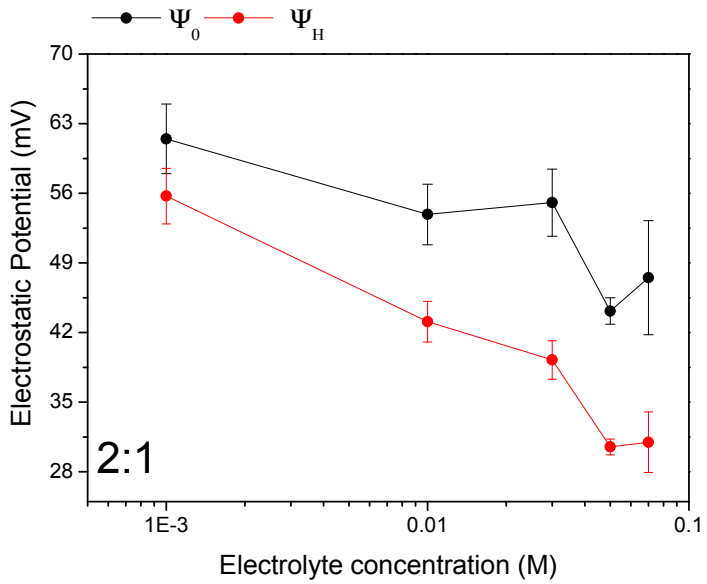

Figure 4.6: Plane Potential(Ψ_0) and Potential at the Helmholtz plane (Ψ_H) as function of electrolyte concentration for a electrolyte 2:1 calculated using a theoretical fitting.

CHAPTER 5

Conclusions and forthcoming research

The main objective of this thesis has been the construction of a reliable experimental and theoretical setup to determine the electrophoretic mobility of colloidal particles.

Such task comprised several stages, viz.:

- The restoration and refurbishing of an aged and inactive optical equipment to measure electrophoretic mobilities (for particles in the range of micrometers). That also included the maintenance of the measurement cell and of the optical and video components attached.

- The calibration of the apparatus and the completion of reliability tests of its resulting values, via comparisons with data provided by alternative laser-based equipments in operation.

- The incorporation of a theoretical protocol, based in the well-known electrokinetic formalism by O'Brien and White, in order to fit the experimental mobilities. Such procedure allows the determination of zeta potentials and/or electrokinetic colloidal charges.

- The realization of a series of preliminary experiments to obtain the mobility of latex and silica particles immersed in univalent electrolyte environments.

The present work has opened a new investigation line of experimental research, which constitutes the first contribution of the University of Sinaloa in this topic. For the performing of the

experimental research we established the first bases of a laboratory of colloids at the Universidad Autónoma de Sinaloa.

As a final example of a very interesting result obtained as a part of this work, we present an evidence of the phenomenon of *reversed* electrophoretic mobility.

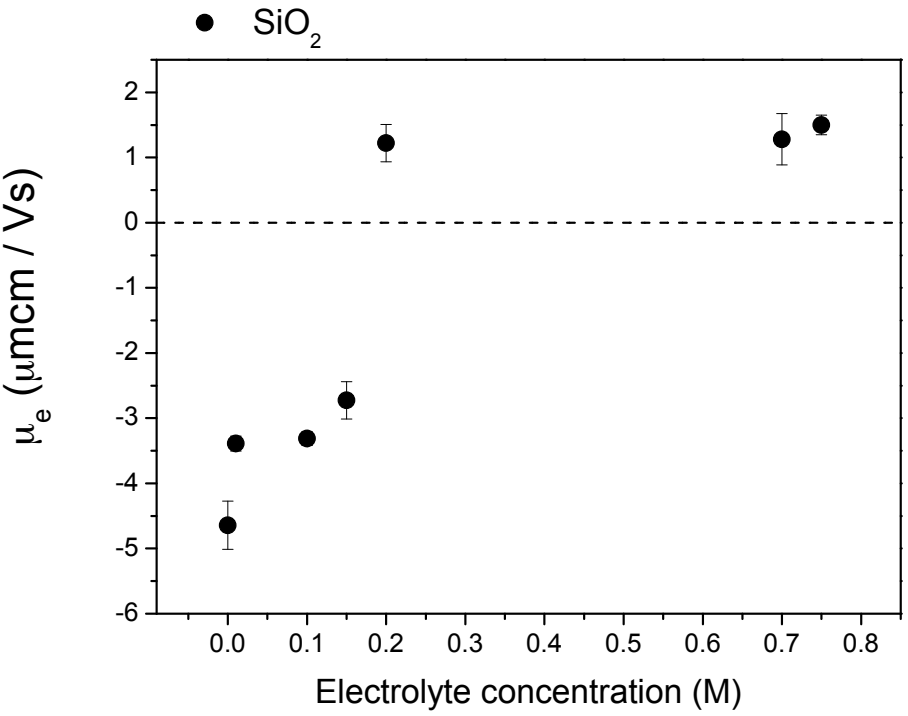

Figure 5.1: Electrophoretic mobility as function of electrolyte concentration (NaCl). The effect known as *reversed* electrophoretic mobility can be observed at electrolyte concentrations higher than 0.2M

Finally, in the near future, we aim to improve and refine our experimental setup, in order to consolidate this technique as one of the bases of a pioneering laboratory in materials science at the Universidad Autónoma de Sinaloa.

We present an alternative to commercial devices for particle imaging, taking into account several aspects: the use of new technologies, straightforward assembling, efficiency, user-friendly interface and low cost. This way, we have performed the assembling of a cheap portable device "The Raspberry Pi microcontroller" system in a conventional microscope. We printed pieces using a 3D printer for the assembly of the Raspberry Pi and the Raspberry Pi Noir camera for images acquisition in a Laborlux S optical microscope (see Figure 5.2)

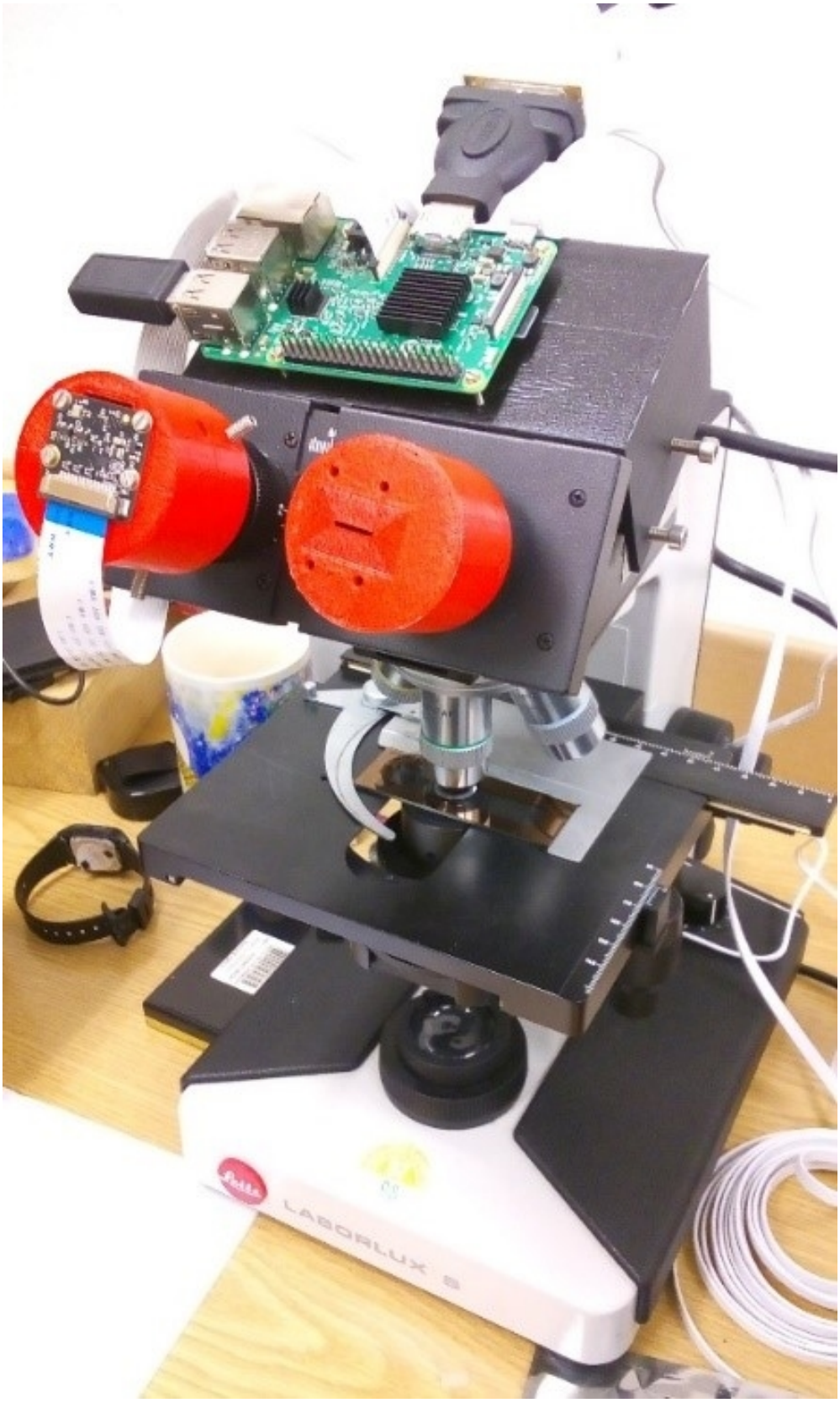

Figure 5.2: Assembly of Raspberry Pi and the Pi Noir camera in the Laborlux S microscope using the 3D printed pieces.

The images of $4\mu m$ PS microparticles acquired with our set up were compared with the obtained with a NIKON confocal microscope which uses an ATV Marlin FT-131 camera to image acquisition. In figure 5.3 the images obtained with the two different set ups are shown. In Figure 5.3 (a) the image was acquired with the Nikon Confocal and Figure 5.3 (b) with our arrangement (conventional microscope and Raspberry Pi).

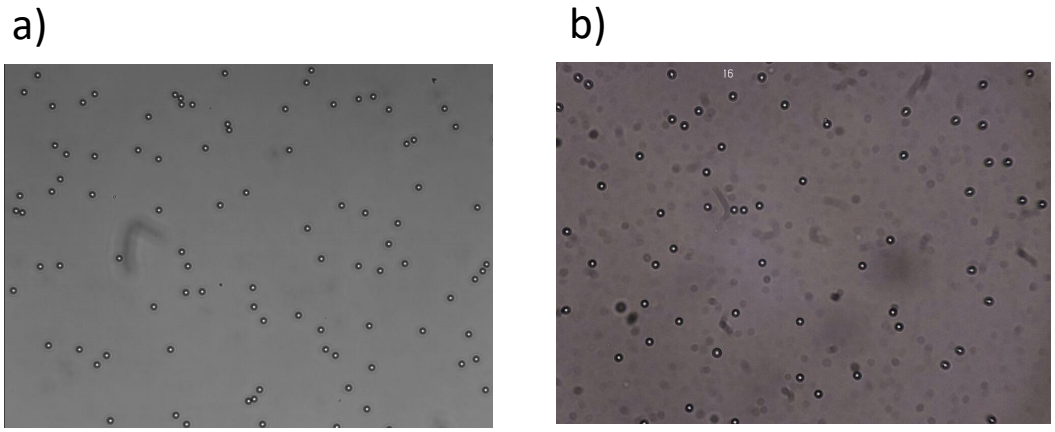

Figure 5.3: Images acquired with a) Nikon confocal microscope with its camera and b) Raspberry Pi Camera module coupled in the Laborlux S conventional microscope to $4\mu m$ PS particles.

Using the experimental set up shown, we would be able to automatize the particle tracking to measure electrophoretic mobility by coupling the Raspberry Pi and its camera to our Zeta meter. On the other hand, and regarding the theoretical aspects of the problem, we plan to make use of modern electrokinetic approaches that embody relaxation and finite-size ionic effects. Notably, such novel formalisms have been able to explain, from first principles, the occurrence of reversed electrophoretic mobilities.

CHAPTER 6

Acknowledgements

Authors are grateful to the Dr. José Luis Arauz Lara and Dra. María de los Ángeles Ramz Saito for experimental research developed at the Instituto de Física, UASLP

The authors also thank to the computer resources, technical expertise and support provided by the Cinvestav-Abacus supercomputer is thankfully acknowledged. The assistance from the computer technicians at the IF-UASLP is also acknowledged.

Bibliography

[1] Hiemenz, P. C.; Rajagopalan, R. *Principles of Colloid and Surface Chemistry, revised and expanded*; CRC press, 1997; Vol. 14.

[2] Hunter, R. Polymeric stabilization and flocculation. *Foundations of colloid science* **1987**, *1*, 450–493.

[3] Russel, W. B.; Saville, D. A.; Schowalter, W. R. *Colloidal dispersions*; Cambridge university press, 1989.

[4] Evans, D. F.; Wennerstrom, H. The colloid domain, where physics, chemistry and biology meet. 1994.

[5] Jiménez-Ángeles, F.; Lozada-Cassou, M. A model macroion solution next to a charged wall: overcharging, charge reversal, and charge inversion by macroions. *The Journal of Physical Chemistry B* **2004**, *108*, 7286–7296.

[6] Quesada-Pérez, M.; González-Tovar, E.; Martín-Molina, A.; Lozada-Cassou, M.; Hidalgo-Álvarez, R. Overcharging in colloids: Beyond the Poisson–Boltzmann approach. *ChemPhysChem* **2003**, *4*, 234–248.

[7] Lyklema, J. Overcharging, charge reversal: chemistry or physics? *Colloids and Surfaces A: Physicochemical and Engineering Aspects* **2006**, *291*, 3–12.

[8] Guerrero-García, G. I.; González-Tovar, E.; Lozada-Cassou, M.; de J. Guevara-Rodríguez, F.

The electrical double layer for a fully asymmetric electrolyte around a spherical colloid: An integral equation study. *The Journal of chemical physics* **2005**, *123*, 034703.

[9] Dukhin, S. S.; Deriaguine, B. V. *Surface and Colloid Science: Electrokinetic Phenomena: Translated from the Russian by A. Mistetsky and M. Zimmerman*; Plenum Press, 1974.

[10] O'Brien, R. W.; White, L. R. Electrophoretic mobility of a spherical colloidal particle. *Journal of the Chemical Society, Faraday Transactions 2: Molecular and Chemical Physics* **1978**, *74*, 1607–1626.

[11] Lozada-Cassou, M.; González-Tovar, E.; Olivares, W. Nonlinear effects in the electrophoresis of a spherical colloidal particle. *Physical Review E* **1999**, *60*, R17.

[12] Lozada-Cassou, M.; González-Tovar, E. Primitive model electrophoresis. *Journal of colloid and interface science* **2001**, *239*, 285–295.

[13] Wiersema, P.; Loeb, A.; Overbeek, J. T. G. Calculation of the electrophoretic mobility of a spherical colloid particle. *Journal of Colloid and Interface Science* **1966**, *22*, 78–99.

[14] Quesada-Pérez, M.; González-Tovar, E.; Martín-Molina, A.; Lozada-Cassou, M.; Hidalgo-Álvarez, R. Ion size correlations and charge reversal in real colloids. *Colloids and Surfaces A: Physicochemical and Engineering Aspects* **2005**, *267*, 24–30.

[15] McQuarrie, D. Statistical Mechanics. 2000. *Sausalito, Calif.: University Science Books* **2004**, *12*, 641.

[16] Hansen, J. P.; McDonald, I. R. Theory of simple liquids. 1960.